Solar Energy Materials & Solar Cells 115 (2013) 21–28

Contents lists available at SciVerse ScienceDirect

Solar Energy Materials & Solar Cells

journal homepage: www.elsevier.com/locate/solmat

A novel method to extract the series resistances of individual cells in a photovoltaic module

Yong Sin Kim [a,c,*], Sung-Mo Kang [b], Bruce Johnston [c], Roland Winston [c]

[a] School of Electrical and Electronics Engineering, Chung-Ang University, Seoul, 156-756, Republic of Korea
[b] College of Information Science & Technology, KAIST, Daejeon, 305-701, Republic of Korea
[c] School of Natural Science, University of California at Merced, Merced, CA. 95343, USA

ARTICLE INFO

Article history:
Received 22 May 2012
Received in revised form
17 March 2013
Accepted 19 March 2013
Available online 16 April 2013

Keywords:
Photovoltaic
Solar cell
Series resistance
I–V curve
Differential resistance
Partial shading

ABSTRACT

Non-disruptive cell-level characterization of a photovoltaic module is presented. Previous works have developed methods to extract the shunt resistances and the short circuit currents of individual cells, but their series resistances have not been characterized yet. In this paper, a novel methodology that quantifies the series resistances of individual cells is developed by using a partial shading technique with two different shading ratios. The simulation and experimental test results are presented for validation.

1. Introducton

The current–voltage (*I–V*) characteristics of solar cells depending on materials and physical configurations are of most important to estimate and to evaluate their performances. Previous works have proposed methods to extract the internal model parameters of a solar cell such as the saturation current [1], the ideality factor [2], the photocurrent [3], the shunt resistance [4], and the series resistance [5,6]. Since solar cells generate high current at low voltages, the series resistances of solar cells lead to significant power loss. Moreover, the recent development of industrial solar cells towards increasing the cell area and the current and results in more losses [5].

Considering *I–V* characteristics of photovoltaic (PV) modules including an assembly of individual solar cells into a single package, extracting the internal parameters of individual solar cells within an encapsulated module without disassembling or disconnecting the internal circuits has been a major challenge. A heat sensing technique using infrared imaging is widely used to locate the defective areas [7], but the thermal information can hardly be converted to the internal parameters. A method using a single cell dark *I–V* curve and the maximum differential resistance d*V*/d*I* characterizes the internal diode and the shunt resistances of individual cells, but some of the light could be come from the top glass and reached to the cells by internal reflection [8]. Authors in [9] have developed the method of extracting the short circuit current and the shunt resistance from the d*V*/d*I* characteristics of individual cells by using a partial shading effect [10]. In [11], individual cell-level *I–V* characteristics of a tandem cell were presented while ignoring the series resistances. Previously discussed techniques to extract the series resistances of solar cells cannot be used to extract the series resistances of individual cells in a module with only two terminals, since individual cells cannot be characterized directly.

This paper presents a novel technique that extracts the series resistances of individual PV cells without disassembling a module by using partial shadings of individual cells and their voltages at the local peak of d*V*/d*I*. The constant light source based *I–V* measurement procedure including qualification, accelerated lifetime, and long-term tests, can be used to analyze the performances and mismatches of PV modules at a cell level for better reliability analysis [12], to model the system including mismatches [13], and to investigate failure mechanisms by detecting degradation spots in a module. Furthermore, the tests performed using only a small number of modules (typically less than 10) can be statistically meaningful by having cell-level parameters [14].

2. Extracting series resistances of individual Cells

To extract the series resistances of individual cells in a PV module, the basic flow is shown in Fig. 1 which begins with

* Corresponding author at: Chung-Ang University, School of Electrical and Electronics Engineering, 84 Heukseok-Ro, Dongjak-Gu, Seoul, 156-756, Republic of Korea. Tel.: +822 823 2309.
E-mail address: shonkim@cau.ac.kr (Y.S. Kim).

0927-0248/$ - see front matter © 2013 Elsevier B.V. All rights reserved.
http://dx.doi.org/10.1016/j.solmat.2013.03.021

1	Characterize the series resistance for a PV module without shading
2	Set one of cells in a module to be shaded partially
3	Characterize d*V*/d*I* of a partially shaded cell
4	Characterize d*V*/d*I* of all other unshaded cells
5	Find the voltage and current of the module at max(dV/dI)
6	Change the value of shading ratio and repeat Steps from 3 to 5
7	Extract the series resistance of unshaded cells
8	Repeat Steps from 2 to 7 for every cell in the module
9	Extract the series resistances of individual cells

Fig. 1. Basic flow of the proposed method to extract the series resistances of individual cells in a module.

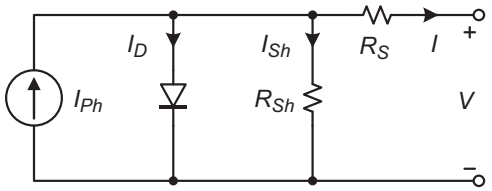

Fig. 2. Equivalent circuit of a PV module.

characterizing the series resistance of a PV module. When a module is composed of N_S cells connected in series and only one of the cells is partially shaded, the operating voltages of unshaded cells and the partially shaded cell can be different depending on the voltage across the module. By having two separate models (one for unshaded cells and the other for the partially shaded cell), the proposed method introduces the way to extract the series resistances of individual cells in a module.

2.1. The series resistance of a PV module (step 1 in Fig. 1)

Since a low voltage is generated by a typical PV cell, conventional modules use PV cells in series to increase the voltage output. The most common model based on a single diode for a PV module is shown in Fig. 2 [6,15]. By using Kirchhoff's current law, the current–voltage (*I*–*V*) relation is given by

$$I = I_{Ph} - I_D - I_{Sh}$$
$$= I_{Ph} - I_0\left\{\exp\left(\frac{V+IR_S}{nV_T}\right)-1\right\} - \frac{V+IR_S}{R_{Sh}} \quad (1)$$

where I is the module current, V the module voltage, I_{Ph} the photocurrent proportional to irradiance, I_D the internal diode current, I_{Sh} the shunt leakage current, I_0 the reverse saturation current of the diode, n the ideality factor, V_T the thermal voltage, R_S the series resistance, and R_{Sh} the shunt resistance. The method to extract the series resistance of a PV cell or module was first introduced in [16] by using *I*–*V* characteristics at two different irradiances. *I*–*V* curves at two different irradiances can be distinguished in two aspects: the first is the difference ΔI_{SC} in two short circuit currents and the second is the smaller voltage drop $\Delta V = R_S \Delta I_{SC}$ by the series resistance at lower irradiance, where the value of R_S is readily obtained [5,16]. ΔV is chosen to be the voltage difference at cross points between the *I*–*V* cures and the fixed current $I = I_{SC} - \Delta I$ so as to obtain points near the knee of the *I*–*V* characteristics. Fig. 3 shows *I*–*V* curves at two different irradiances and the method to choose ΔI according to the international standard IEC 6089 [17]. In this case, ΔI is set to the current difference between the short circuit I_{SC1} and the current at the maximum power point P_{MP1} from the one sun *I*–*V* curve. The same ΔI is applied to the 0.5 sun *I*–*V* curve, and the corresponding voltage $V_{MP1}+\Delta V$ is obtained at the current $I_{SC2}-\Delta I$. Then the

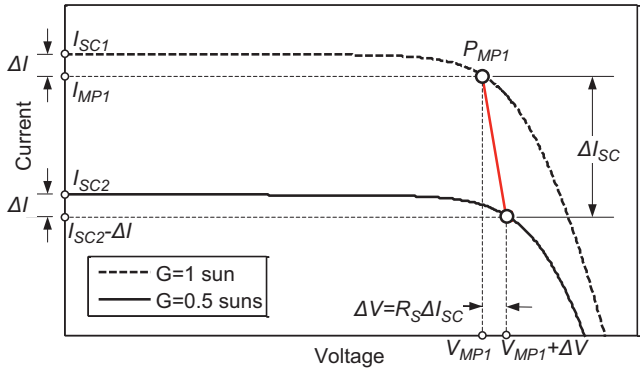

Fig. 3. Extraction of the series resistance from *I*–*V* curves of a PV module at two different irradiances.

extracted series resistance R_S becomes

$$R_S = |\Delta V / \Delta I_{SC}| \quad (2)$$

2.2. The differential resistance of a partially shaded cell (steps 2 and 3 in Fig. 1)

When the *i*th cell in a module becomes the only cell shaded, the current through the module is dictated by the shaded cell (i.e. $I = I(i)$). Based on an assumption that the photocurrent of a partially shaded cell is proportional to the unshaded area at a given irradiance, the cell current $I(i)$ through the *i*th cell can be expressed as

$$I(i) = (1-SR)I_{Ph}(i) - I_0\left\{\exp\left(\frac{V(i)+I(i)R_S(i)}{nV_T}\right)-1\right\} - \frac{V(i)+I(i)R_S(i)}{R_{Sh}(i)} \quad (3)$$

where SR is a shading ratio indicating the area shaded to the area of the cell and R_{Sh} is the shunt resistance. $X(i)$ represents the property of X for the *i*th cell. The lumped series resistance R_S and the module voltage V can be expressed as the sum of their individual cell properties as

$$R_S = \sum_i R_S(i) = R_S(i) + R_S^C(i) \quad \text{and} \quad V = \sum_i V(i) = V(i) + V^C(i) \quad (4)$$

where each variable with superscript C represents the complementary of its own variable in a module. In other words, $R_S^C(i)$is the series resistance of a module excluding the shaded cell. The same applies to $V^C(i)$.

The differential resistance $dV(i)/dI(i)$ of a partially shaded cell can be expressed, similar to that shown in [15], as

$$\frac{dV(i)}{dI(i)} = -\left\{\frac{1}{nV_T}\left((1-SR)I_{Ph}(i) - I(i) + I_0 - \frac{V(i)+I(i)R_S(i)}{R_{Sh}(i)} + \frac{nV_T}{R_{Sh}(i)}\right)\right\}^{-1} - R_S(i) \quad (5)$$

To find the maximum value of $dV(i)/dI(i)$, let X be

$$X = \frac{1}{nV_T}\left((1-SR)I_{Ph}(i) - I(i) + I_0 - \frac{V(i)+I(i)R_S(i)}{R_{Sh}(i)} + \frac{nV_T}{R_{Sh}(i)}\right) \quad (6)$$

then second derivative of $V(i)$ that gives maximum $dV(i)/dI(i)$ can be expressed as

$$\frac{d^2V(i)}{dI(i)^2} = X^{-2}\frac{1}{nV_T}\left(-1 + \frac{1}{R_{Sh}(i)}X^{-1}\right) = 0 \quad (7)$$

which makes the solution $X = 1/R_{sh}(i)$, then $V(i)$ can be obtained as

$$V(i) = R_{Sh}(i)(1-SR)I_{Ph}(i) + R_{Sh}(i)I_0 - I(i)(R_S(i) + R_{Sh}(i)) \quad (8)$$

The current at the maximum value of $dV(i)/dI(i)$ is proportional to the short circuit current as discussed in [9] and can be defined as

$$I(i) = (1-SR)I_{SC}(i) + \alpha \quad (9)$$

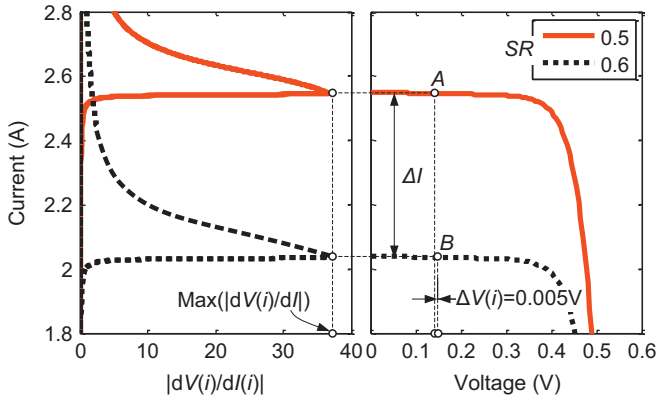

Fig. 4. The differential resistance and *I–V* curve of a partially shaded PV cell with two different shading ratios (SR_A=0.5 and SR_B=0.6).

Table 1
Model parameters for a module.

Parameters	Values
Average series resistance (R_S)	10 mΩ
Average shunt resistance (R_{Sh})	40Ω
Junction breakdown voltage (V_{Br})	−8 V
Fraction of shunt current involve in breakdown (a)	0.5
Avalanche breakdown exponent (m)	3.7

where $I_{SC}(i)$ is the short circuit current of the ith cell that can be derived from Eq. (3) at $V(i)=0$ and $SR=0$. Here α is a constant. Applying two different values of the shading ratios SR_A and SR_B (where $SR_A < SR_B$) to Eq. (9) at each current $I_A(i)$ and $I_B(i)$, respectively, and subtracting one from another give

$$\Delta I(i) = I_A(i) - I_B(i) = (SR_B - SR_A) I_{SC}(i) \tag{10}$$

$\Delta V(i)$ can be derived from Eqs. (8) and (9) as

$$\Delta V(i) = V_A(i) - V_B(i) = (SR_B - SR_A) R_{Sh}(i) \{ I_{Ph}(i) - I_{SC}(i)(1 + R_S(i)/R_{Sh}(i)) \} \tag{11}$$

It indicates that the voltage difference $\Delta V(i)$ for SR_A and SR_B at maximum $dV(i)/dI$ (i) is less likely to be affected by shading ratio, since the different between $I_{Ph}(i)$ and $I_{SC}(i)$ is small and $R_{Sh}(i) \gg R_S(i)$. Fig. 4 shows *I–V* curves of two different shading ratios SR_A=0.5 and SR_B=0.6 with all the parameters from Table 1. The right hand side figure indicates that the open circuit voltage decreases as the shading ratio increases. However, the variation of maximum $dV(i)/dI(i)$ in terms of the shading ratio is negligible as can be seen from the left hand side figure, and the voltage difference ΔV at maximum $dV(i)/dI(i)$ points is less than 0.1% of its own open circuit voltage without shading. As only one of the cells in a module is partially shaded, the shaded cell can be negatively biased at the current value higher than $(1-SR)I_{Ph}(i)$. For accurate analysis of the differential resistance, Eq. (3) can be modified based on the PVNET and PVSIM model in [18,19]. In this case, the shunt leakage current $I_{Sh}(i)$ of a partially shaded cell in Eq. (1) can be modeled as the sum of the current through the shunt resistance $R_{Sh}(i)$ and non-linear current with the multiplication exponent m by avalanche breakdown as shown in Fig. 5, and it can be expressed as

$$I_{Sh}(i) = \frac{V(i) + I(i)R_S(i)}{R_{Sh}(i)} \left\{ 1 + a \left(1 - \frac{V(i) + I(i)R_S(i)}{V_{Br}} \right)^{-m} \right\} \tag{12}$$

where a the fraction of shunt current involved in breakdown and V_{Br} the junction breakdown voltage.

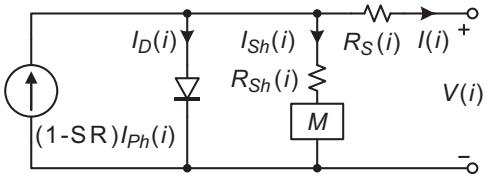

Fig. 5. Equivalent circuit of a partially shaded PV cell with a non-linear multiplication factor.

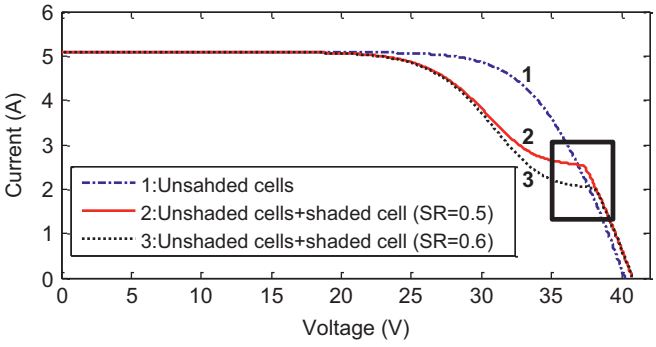

Fig. 6. Simulated *I–V* curves for N_S−1 unshaded cells with or without a partially shaded cell at two different shading ratio (SR_A=0.5 and SR_A=0.6).

2.3. The differential resistance of all other unshaded cells in series (step 4 in Fig. 1)

Considering all other unshaded cells excluding the partially shaded ith cell in a module, the *I–V* relationship of a lumped model based on Eq. (1) becomes

$$I^C(i) = I(i) = I_{Ph}(i) - I_0 \left\{ \exp\left(\frac{V^C(i) + I(i)R_S^C(i)}{nV_T(N_S-1)} \right) - 1 \right\} - \frac{V^C(i) + I(i)R_S^C(i)}{R_{Sh}^C(i)} \tag{13}$$

The voltage $V^C(i)$ across the unshaded cells meets $V^C(i) = V - V(i)$ where V is the voltage across a module. Eq. (13) can be rewritten as voltage form, which is

$$V^C(i) = nV_T(N_S-1) \left\{ \ln\left(I_{Ph}(i) - I(i) + I_0 - \frac{V^C(i) + I(i)R_S^C(i)}{R_{Sh}^C(i)} \right) - \ln(I_0) \right\} - I(i)R_S^C(i) \tag{14}$$

The differential resistance of the N_S−1 unshaded cells can be expressed as

$$\frac{dV^C(i)}{dI(i)} = -\left\{ \frac{1}{nV_T(N_S-1)} \left(I_{Ph}(i) - I(i) + I_0 - \frac{V^C(i) + I(i)R_S^C(i)}{R_{Sh}^C(i)} + \frac{nV_T(N_S-1)}{R_{Sh}^C(i)} \right) \right\}^{-1} - R_S^C(i) \tag{15}$$

2.4. The series resistances of individual cells in a module (Steps 5–9 in Fig. 1)

Fig. 6 depicts the *I–V* curves of N_S−1 unshaded cells (indicated as "1") and a module with a partially shaded cell for different shading ratios SR=0.5 and 0.6 (indicated as "2" and "3"). As discussed in [8], *I–V* curves of a module with a partially shaded cell exhibits a "kink" that corresponds to the current at which the shaded cell dictates the module current and becomes reverse biased. The differential resistance of a module including a partially shaded cell can be obtained from Eqs. (5) and (15) as

$$\frac{dV}{dI} = \frac{d\left(V(i) + V^C(i)\right)}{dI(i)} = \frac{dV(i)}{dI(i)} + \frac{dV^C(i)}{dI(i)} \tag{16}$$

Considering only the current range represented as a box in Fig. 6, where all the bypass diodes remain in the off state, the internal diode current through the unshaded cells becomes dominant as the voltage increases. Figs. 7 and 8 show the close-up view of the box area in Fig. 6 for the differential resistance of the module in terms of output current and voltage, where the numbers are indicating the same contents as shown in Fig. 6. The differential resistance $dV^C(i)/dI(i)$ of unshaded cells is monotonic with respect to voltage and is much smaller than $dV(i)/dI(i)$ of a shaded cell. Assuming that the current through unshaded cells is linear to the voltage in this range, the second derivative can be approximated as

$$\frac{d^2V}{dI^2}=\frac{d^2V(i)}{dI(i)^2}+\frac{d^2V^C(i)}{dI(i)^2}\approx\frac{d^2V(i)}{dI(i)^2} \tag{17}$$

The short circuit currents I_A and I_B of a shaded cell at SR_A and SR_B can be defined as the cross-points A from curves 1 and 2 and B from curves 1 and 3, respectively. Since the maximum value of dV/dI for a module with a shaded cell is proportional to the short circuit current of the shaded cell as discussed from Eqs. (7)–(9), line AB can be approximated to be parallel to line $A'B'$ where the points A' and B' can be obtained from the I–V curves that meet

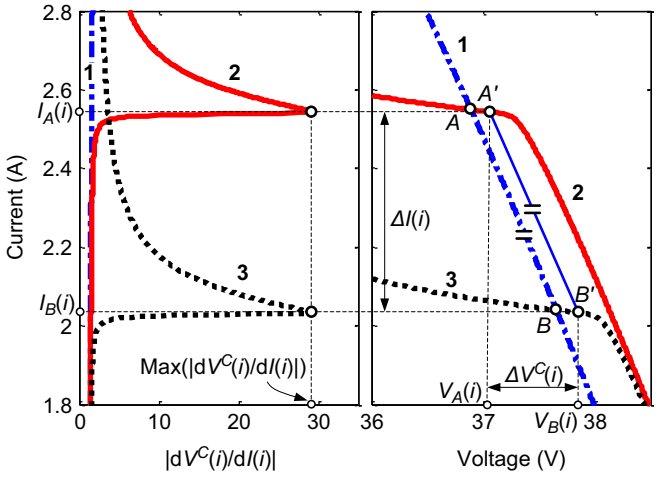

Fig. 7. Close-up view of Fig. 6 (right) and the module current according to the differential resistance (left).

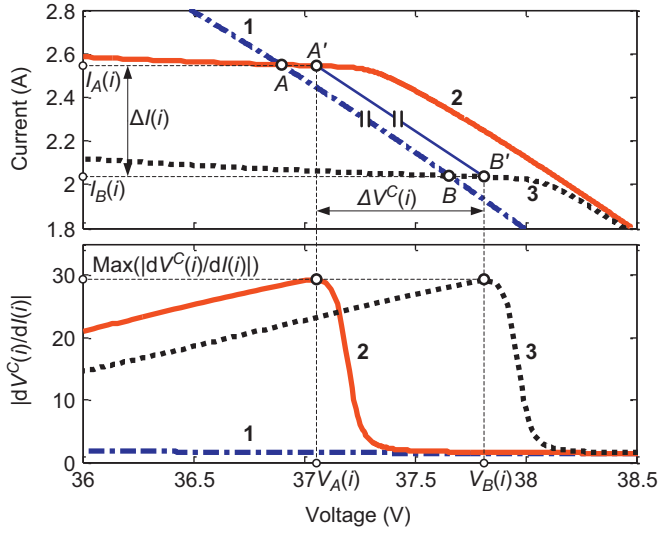

Fig. 8. Close-up view of Fig. 6 (top) and the differential resistance in terms of the output voltage (bottom).

$d^2V/dI^2=0$. Then the series resistance of unshaded cells $R_S^C(i)$ can be defined as

$$R_S^C(i)=R_S-R_S(i)=\Delta V^C(i)/\Delta I(i) \tag{18}$$

where $\Delta V^C(i)$ and $\Delta I(i)$ can be extracted from points A' and B'. In order to consider offsets in $R_S^C(i)$, $R_S^C(i)$ can be modified as

$$R_S^C(i)=\beta\left(\frac{\Delta V^C(i)}{\Delta I(i)}-\overline{\frac{\Delta V^C(i)}{\Delta I(i)}}\right)+\gamma\overline{\frac{\Delta V^C(i)}{\Delta I(i)}} \tag{19}$$

where $\bar{x}$ represents the mean of x. β and γ are two variables to be decided. Then, the summation of $R_S^C(i)$ from $i=1$ to $i=N_S$ becomes

$$\sum_{i=1}^{N_S}R_S^C(i)=(N_S-1)R_S=\beta\sum_{i=1}^{N_S}\frac{\Delta V^C(i)}{\Delta I(i)}+(-\beta+\gamma)N_S\overline{\frac{\Delta V^C(i)}{\Delta I(i)}} \tag{20}$$

where R_S can be extracted from Eq. (2). Another equation can be obtained by limiting $R_S^C(i)$ as $\max\left(R_S^C(i)\right)\approx R_S$ which gives

$$R_S\approx-\beta\max\left(\frac{\Delta V^C(i)}{\Delta I(i)}\right)+(-\beta+\gamma)\overline{\frac{\Delta V^C(i)}{\Delta I(i)}} \tag{21}$$

The series resistance of ith cell in a module can be obtained after acquiring each $R_S^C(i)$, β, and γ as

$$R_S(i)=R_S-R_S^C(i) \tag{22}$$

3. Simulation results

Considering two different irradiances to extract the series resistance of a PV module, one was set to be a standard testing condition at irradiance $G_0=1000\ W/m^2$ and $T=25\ ^\circ C$. We varied the irradiance G for the other, simulated I–V characteristics, and extracted the series resistances. Fig. 9 shows error between the original value of the series resistance and the extracted one, which indicates errors within $\pm 1\%$ for the range of G/G_0 from 0.35 to 0.9. The error in extracting the series resistance can be minimized around the value of $G/G_0=0.5$

When a single cell is partially shaded, the current at the maximum value of dV/dI is proportional to the short circuit current I_{SC} under normal operation at the rate of $(1-SR)$ as shown in Eq. (9). Fig. 10 shows the current at the maximum value of dV/dI, $(1-SR)I_{SC}$, and their offset α which is three orders of magnitude lower than the current value throughout the full range of shading ratio. However, this small current offset can cause a large voltage variation depending on the value of shunt resistance and shading ratio. Various values of the shunt resistance $R_{Sh}(i)$ (from 20 to 60 Ω) were simulated as depicted in Fig. 11 to investigate the variations of the current and voltage at the maximum dV/dI. The current variation for various values of the shunt resistance at a given shading ratio is negligible compared to the voltage variation. Thus, two shading ratios need to be chosen close enough to

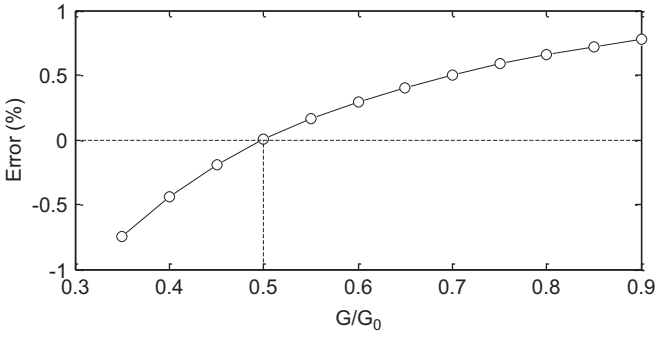

Fig. 9. Error in extracting the series resistance of a module with various values of irradiance G.

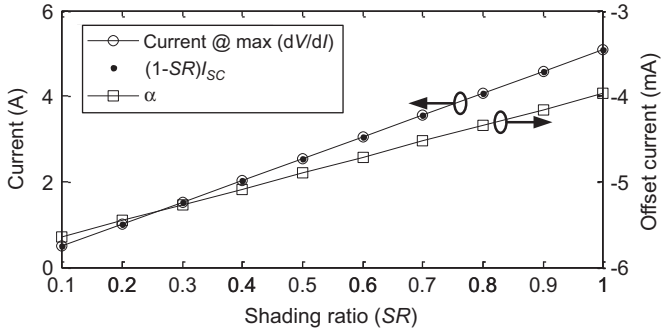

Fig. 10. Current at the maximum value of dV/dI proportional to (1−SR)I_{SC} and its offset α from (1−SR)I_{SC}.

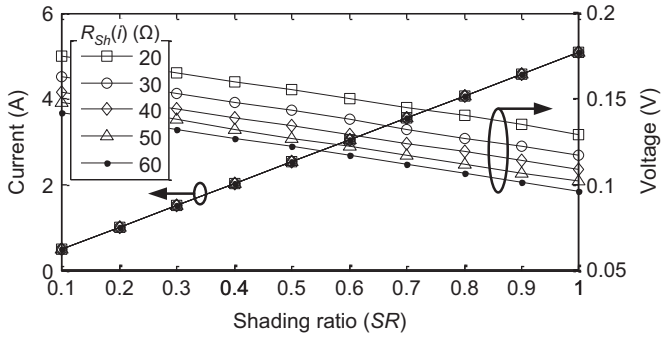

Fig. 11. Current and voltage at the maximum value of dV/dI with various values of $R_{Sh}(i)$.

neglect the variation. As can be seen in Figs. 7 and 8, however, the closer the two shading ratios SR_A and SR_B (where $SR_A < SR_B$) are, the less the current and voltage differences ($\Delta I(i)$ and $\Delta V^C(i)$) are. To keep error in extracting the series resistance of unshaded cells within a certain level in the presence of noise and parameter variations under real testing conditions, $\Delta I(i)$ and $\Delta V^C(i)$ need to be decided based on the minimum resolutions of current and voltage sensors. If the value of SR_A becomes closer to zero (an unshaded condition), neither the current–voltage of unshaded cells can be assumed to be linear nor d^2V/dI^2 in Eq. (17) is dominated by a shaded cell. On the other hand, as SR_B gets closer to one (a completely shaded condition), not only does the signal to noise ratio increase but also the possibility that defects exist under the shaded area of a cell. It may increase the error in reading the output current dictated by the shaded cell. Thus, SR_A and SR_B are chosen to be 0.5 and 0.6 for the simulation, respectively.

Based on the mean values of parameters in Table 1, the series resistances and the shunt resistances of individual cells are generated from normal distributions with standard variations 20% of their own mean values as shown in Fig. 12. By using Eq. (19), the series resistances of unshaded cells $R_S^C(i)$ with ith cell partially shaded are extracted and compared with the generated values as shown in Fig. 13. Considering the linear curve fit, the extracted values can be considered proportional to the generated values with a small mismatch. The values of β and γ allow extracted values $R_S^C(i)$ to fit the generated values and are obtained as $\beta=0.46$ and $\gamma=2.01$ with less than 1% error. However, this error strongly depends on the resolution of a data acquisition system. From Eq. (22), the series resistances of individual cells can be extracted as depicted in Fig. 14. Fig. 15 shows the maximum and the average errors in extracting the series resistances of individual cells according to the number of bits in floats for both current and voltage sensing. The more accurate the data acquisition system is, the less the error we acquire. An additional simulation for some cells having much higher values of $R_S(i)$ as shown in Fig. 16(a)

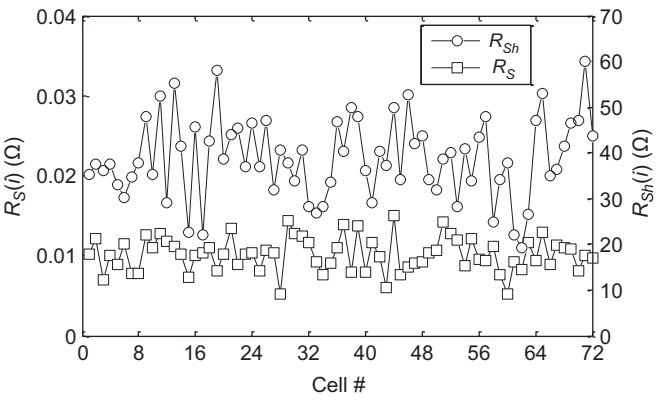

Fig. 12. Normally distributed series resistances and shunt resistances of individual cells with mean 0.01 Ω and 40 Ω, respectively.

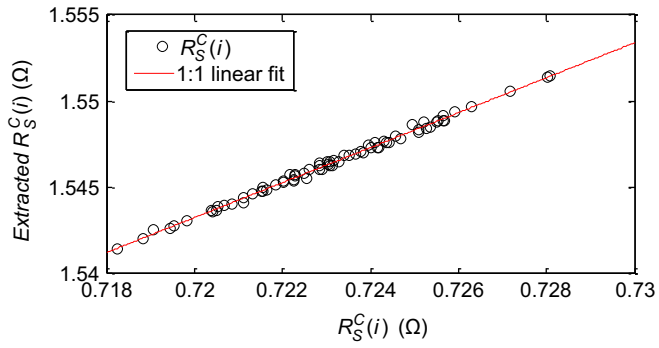

Fig. 13. Simulation results for extracting the series resistances of unshaded cells by using proposed method.

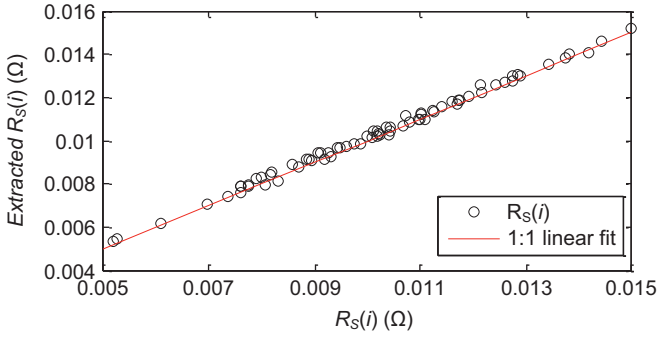

Fig. 14. Simulation results for extracting the series resistances of individual cells by using proposed method.

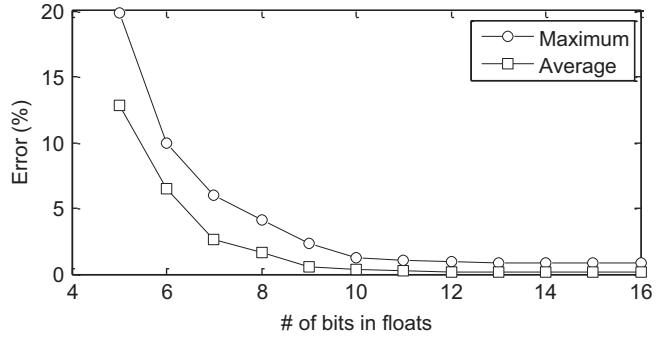

Fig. 15. Maximum and average errors in extracting the series resistance of individual cells according to the number of bits in floats for a data acquisition system.

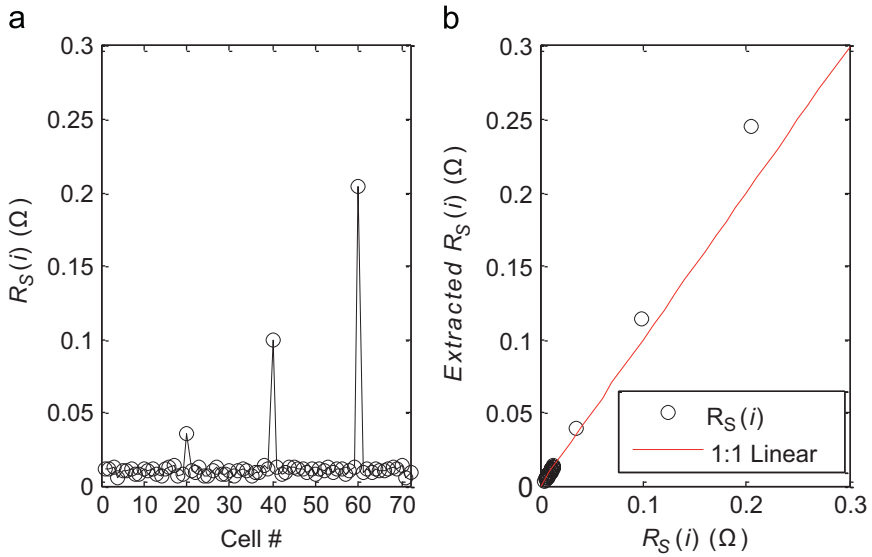

Fig. 16. Simulation results for extracting the series resistances of individual cells. (a) Three cells are set to have much higher values than others (b) Extracted values.

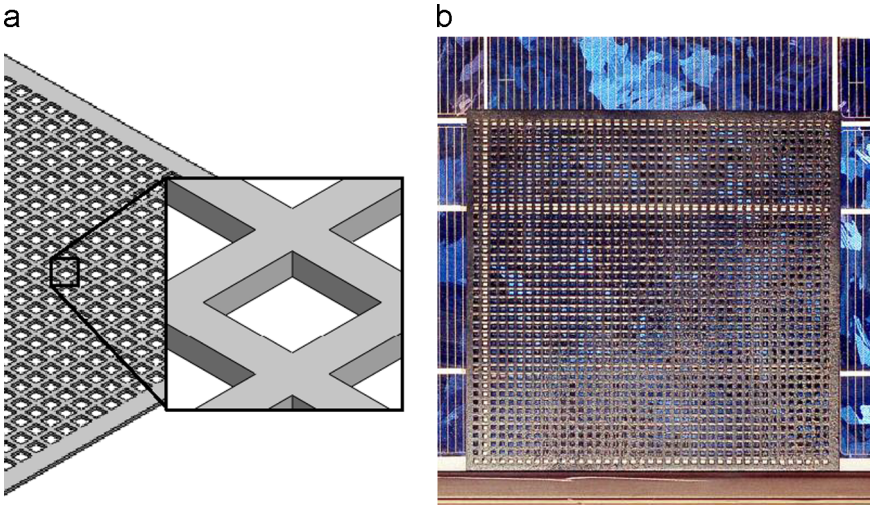

Fig. 17. Mesh screen used in the proposed method for partial shading (a) 3 D rendering (b) Mesh screen by 3D printing placed on top of a cell.

demonstrates an example of damaged cells. We assumed that individual cells initially exhibit 20% variations of the series and the shunt resistances from their average values. Then, three cells are set to have their values 5, 10, and 20 times higher than their initial ones. By using the proposed method, these three values were in good agreement with the extracted values as indicated in Fig. 16(b). However, as the value of $R_S(i)$ increases, the lines AB and $A'B'$ in Figs. 7 and 8 are less likely to be parallel which causes higher extraction error.

4. Test results

The shading ratios $SR_A=0.5$ and $SR_B=0.6$ were precisely controlled by using mesh screens and 3D printing as shown in Fig. 17. The advantages of a mesh screen are inexpensive fabrication and easy shaping. Also the spectrum of the light source is not affected by the screen. The shading ratio is determined by the masked area to the area of a cell, which makes the proposed mesh screen insensitive to positioning and alignment variation as long as the shading ratio retains its value. The size of the mesh screen is custom fit to the size of a cell (here 5in by 5in) in a module with an array of 2 mm by 2 mm holes. Partial shading of a cell was implemented manually by putting a screen on top of the cell, which was the most time consuming part of the test.

A 5 year-old PV module with 72 cells connected in a series was located on a dual-axis tracker for outdoor testing as shown in Fig. 18. Controls and sensors were developed based on a CompactRIO system. The PV module was tested twice on a sunny day under $\pm$ 1% variation of irradiance. The run time of both tests was under 15 min. To minimize the damage to the module by partial shading, the module was initially set as normally open and characterized by a capacitor load I–V curve tracer for a short amount of time at 5 kS/s sampling speed with 1000 samples [20]. The test procedures are as follows.

- Measure R_S of the module: Eq. (2).
- Obtain I–V curves at both shading ratio $SR=0.5$ and 0.6 for each cell: Eqs. (3) and (13)
- Filter noise from I–V curves
- Extract $R_S^C(i)$ for each cell: Eqs. (18) and (19).
- Obtain the values of β and γ: Eqs. (20) and (21).
- Calculate $R_S(i)$ for each cell: Eq. (22).

The measured series resistance of the tested module R_S was 1.38 Ω. When obtaining the I–V curves of a cell partially

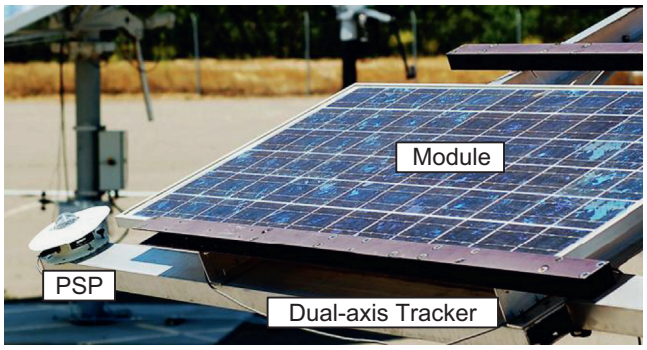

Fig. 18. A test module located on a dual-axis tracker to reduce the variation of irradiance onto the module.

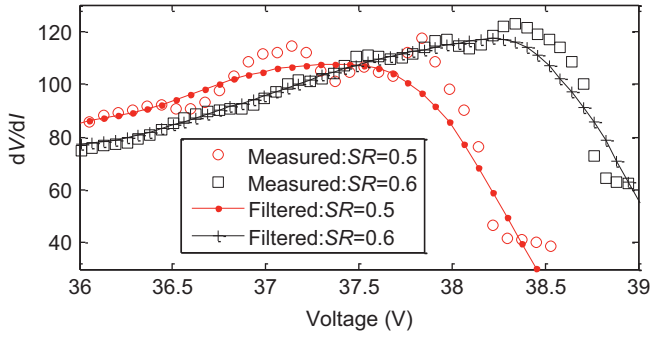

Fig. 19. Experimental results for the differential resistance dV/dI of a PV module with a cell partially shaded at shading ratios 0.5 and 0.6.

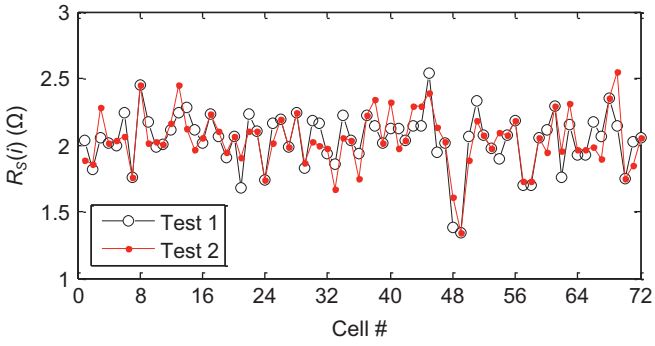

Fig. 20. Experimental results for extracting the series resistances of unshaded cells by using proposed method with two different tests.

shaded, it is important to keep the uniform irradiance condition for both shading ratios due to ΔI in Eq. (18) directly affected by the irradiance change. Automatic positioning of the screen can be used to reduce the run time and irradiance variation in each iteration. Since the differential resistance dV/dI is sensitive to sampling noise, noise reduction filter using weighted linear lease squares and 1st degree polynomial model in Matlab was applied to dV/dI from each I–V curve as shown in Fig. 19. Fig. 20 depicts extracted $R_S^C(i)$ for each cell. β=0.667 and γ=0.042 are obtained from Eqs. (20) and (21).

The distributions of the series resistances of individual cells $R_S(i)$ for two tests are shown in Fig. 21 with a straight line indicating a 1:1 linear fit. Considering the minimum resolution of voltage (34 mV) and current (11 μA) of the test sensors, the average error as shown Fig. 15 can be assumed little more than 12% at 5 bits in floats. However, the characterization error of the proposed method cannot be obtained without disassembling a PV module, thus, the average discrepancy is defined from two

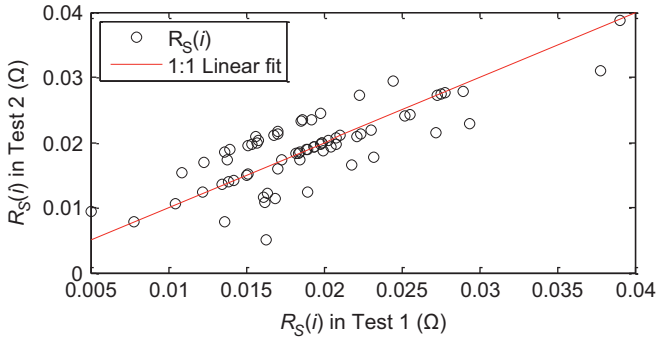

Fig. 21. Distribution of the series resistances of individual cells for two different tests. The solid lines represent 1:1 linear fit of two tests.

separated tests as

$$\text{Discrepancy} = \frac{\overline{|R_S(i)_1 - R_S(i)_2|}}{\max(R_S(i)_1, R_S(i)_2)} \times 100 \approx 13\% \quad (26)$$

where $R_S(i)_1$ and $R_S(i)_2$ represent the series resistance of the ith cell obtained from test 1 and test 2, respectively. Both two tests exhibit a good agreement with the average discrepancy of 13%. It can be expected that the discrepancy of the proposed test can be reduced if the minimum voltage step decreases by having a highly accurate voltage sensor. Note that the proposed method inherently accumulates noise by summing individual series resistance to obtain the calibration coefficient. It is highly recommended that a test sample with an obvious error is either removed or retested.

5. Relationship of parameters to properties of materials

The performance (especially for fill factor) of a PV cell depends on various parameters such as the series and shunt resistance, reverse saturation current, the diode ideality factor, and the photocurrent. Authors in [8–11] have developed non-disruptive methods to extract some distributed properties of a PV module in a cell-level, since those properties are distributed over the module area and cannot be treated as a simple lumped circuit model. It is known that the fill factor of a PV cell decreases by roughly 2.5% as the series resistance increases by 0.1 Ω [21]. Thus, knowing the series resistance of each cell is of most important to quantify cell-level performance in a module. The proposed scheme presents a non-disruptive methodology to extract the series resistances of individual cell in a PV module. Rather than using a complicated model in [22], the proposed scheme uses distribution model in a cell-level to account for all material properties including the base bulk resistance, the base contact resistance, the emitter sheet resistance, and the electrode resistance.

The degradation of PV cells under long-term continuous illumination occurs by a rapid decrease of the fill factor which is correlated with increase in the series resistance [23]. Cell-level analysis without encapsulation has been studied in [24], which leads to a big difference from real application conditions with physical deterioration of encapsulation [25]. Experimental studies on degradation of PV modules in [26] considered measuring the series resistance increase of PV modules, but it only allowed module-level analysis. The propose scheme analyzes the degradation of individual cells in an encapsulated PV module by extracting the series resistances of individual cells.

PV modules undergo accelerated aging tests as part of certification procedure that would strongly reduce their lifetime in the field. Cracks, micro-cracks, or broken metal fingers in silicon wafer PV cells affect power output. Currently electroluminescence (*EL*) imaging is generally applied to identify spatial distribution of

these defects [27,28]. The proposed scheme has advantage over *EL* imaging by quantifying the exact amount of the increase in the series resistances of individual cells. In conjunction with other cell-level analysis, the proposed scheme enables a complete analysis and experimental studies on cell-level performances including mismatch and shading effects [29,30].

6. Conclusions

We introduced a novel test procedure to characterize the series resistances of individual cells in a PV module without disassembling a module or requiring cell level contacts. The proposed procedure can be applied to the qualification test, accelerated lifetime test, and long-term test of PV modules using *I–V* characteristics with a constant light source for more efficient reliability analysis. Furthermore, it can be used as a screening test to investigate known and unknown failures at a cell level, resulting in reduced test time and cost. Test results validated the accuracy of the proposed test procedure that the discrepancy of two different test results was well controlled.

Acknowledgment

This work was supported in part by the California Energy Commission under Grant PIR-07-016.

References

[1] N. Ravindra, B. Prasad, Saturation current in solar cells: an analysis, Solar Cells 2 (1980) 109–113.
[2] N. Santakrus Singh, A. Jain, A. Kapoor, Determination of the solar cell junction ideality factor using special trans function theory (STFT), Solar Energy Materials and Solar Cells 93 (2009) 1423–1426.
[3] F. Pelanchon, P. Mialhe, J. Charles, The photocurrent and the open-circuit voltage of a silicon solar cell, Solar Cells 28 (1990) 41–55.
[4] M. Lal, S. Singh, et al., A new method of determination of series and shunt resistances of silicon solar cells, Solar Energy Materials and Solar Cells 91 (2007) 137–142.
[5] D. Pysch, A. Mette, S. Glunz, A review and comparison of different methods to determine the series resistance of solar cells, Solar Energy Materials and Solar Cells 91 (2007) 1698–1706.
[6] D. Polverini, G. Tzamalis, H. Müllejans, A validation study of photovoltaic module series resistance determination under various operating conditions according to IEC 60891, Progress in Photovoltaics: Research and Applications 20 (2012) 650–660.
[7] A. Skoczek, T. Sample, E.D. Dunlop, The results of performance measurements of field-aged crystalline silicon photovoltaic modules, Progress in Photovoltaics: Research and Applications 17 (2009) 227–240.
[8] L. De Bernardez, R. Buitrango, Dark *I–V* curve measurement of single cells in a photovoltaic module, Progress in Photovoltaics: Research and Applications 14 (2006) 321–327.
[9] G. Alers, J. Zhou, C. Deline, P. Hacke, S. Kurtz, Degradation of individual cells in a module measured with differential IV analysis, Progress in Photovoltaics: Research and Applications 19 (2011) 977–982.
[10] H. Patel, V. Agarwal, MATLAB-based modeling to study the effects of partial shading on PV array characteristics, IEEE Transactions on Energy Conversion 23 (2008) 302–310.
[11] S.R. Kurtz, K. Emery, J.M. Olson, Methods for analysis of two-functional, two-terminal photovoltaic devices, in: Proceedings of the Twenty Fourth Conference Record on Photovoltaic Energy Conversion 1994, IEEE Photovoltaic Specialists Conference 1994, IEEE First World Conference 1994, pp. 1733–1737.
[12] F. Spertino, J.S. Akilimali, Are manufacturing-mismatch and reverse currents key factors in large photovoltaic arrays? IEEE Transactions on Industrial Electronics 56 (2009) 4520–4531.
[13] Y.S. Kim, S.-M. Kang, R. Winston, Modeling of a concentrating photovoltaic system for optimum land use, Progress in Photovoltaics: Research and Applications 21 (2013) 240–249.
[14] C. Osterwald, T. McMahon, History of accelerated and qualification testing of terrestrial photovoltaic modules: a literature review, Progress in Photovoltaics: Research and Applications 17 (2009) 11–33.
[15] Q. Jia, W.A. Anderson, E. Liu, S. Zhang, A novel approach for evaluating the series resistance of solar cells, Solar Cells 25 (1988) 311–318.
[16] M. Wolf, H. Rauschenbach, Series resistance effects on solar cell measurements, Advanced Energy Conversion 3 (1963) 455–479.
[17] Photovoltaic devices—Procedures for temperature and irradiance corrections to measure *I–V* haracteristics, CEI/IEC 60891, 2009.
[18] J. Bishop, Computer simulation of the effects of electrical mismatches in photovoltaic cell interconnection circuits, Solar Cells 25 (1988) 73–89.
[19] D.L. King, J.K. Dudley, W.E. Boyson, PVSIM: a simulation program for photovoltaic cells, modules, and arrays, in: Proceedings of the Photovoltaic Specialists Conference, 1996., Conference Record of the Twenty Fifth IEEE, 1996: pp. 1295–1297.
[20] E. Durán, M. Piliougine, M. Sidrach-de-Cardona, J. Galán, J. Andújar, Different methods to obtain the *I–V* curve of PV modules: a review, in: Photovoltaic Specialists Conference, 2008. PVSC'08. 33rd IEEE, 2008: pp. 1–6.
[21] M. Dadu, A. Kapoor, K. Tripathi, Effect of operating current dependent series resistance on the fill factor of a solar cell, Solar Energy Materials and Solar Cells 71 (2002) 213–218.
[22] M.-K. Lee, J.-C. Wang, S.-F. Horng, H.-F. Meng, Extraction of solar cell series resistance without presumed current-voltage functional form, Solar Energy Materials and Solar Cells 94 (2010) 578–582.
[23] E. Voroshazi, B. Verreet, T. Aernouts, P. Heremans, Long-term operational lifetime and degradation analysis of P3HT: PCBM photovoltaic cells, Solar Energy Materials and Solar Cells 95 (2011) 1303–1307.
[24] K. Kawano, R. Pacios, D. Poplavskyy, J. Nelson, D.D. Bradley, J.R. Durrant, Degradation of organic solar cells due to air exposure, Solar Energy Materials and Solar Cells 90 (2006) 3520–3530.
[25] C. Dechthummarong, B. Wiengmoon, D. Chenvidhya, C. Jivacate, K. Kirtikara, Physical deterioration of encapsulation and electrical insulation properties of PV modules after long-term operation in Thailand, Solar Energy Materials and Solar Cells 94 (2010) 1437–1440.
[26] T. Takashima, J. Yamaguchi, K. Otani, T. Oozeki, K. Kato, M. Ishida, Experimental studies of fault location in PV module strings, Solar Energy Materials and Solar Cells 93 (2009) 1079–1082.
[27] P. Chaturvedi, B. Hoex, T.M. Walsh, Broken metal fingers in silicon wafer solar cells and PV modules, Solar Energy Materials and Solar Cells 108 (2013) 78–81.
[28] S. Kajari-Schröder, I. Kunze, U. Eitner, M. Köntges, Spatial and orientational distribution of cracks in crystalline photovoltaic modules generated by mechanical load tests, Solar Energy Materials and Solar Cells 95 (2011) 3054–3059.
[29] M. Alonso-Garcia, J. Ruiz, F. Chenlo, Experimental study of mismatch and shading effects in the *I–V* characteristic of a photovoltaic module, Solar Energy Materials and Solar Cells 90 (2006) 329–340.
[30] Y.S. Kim, S.-M. Kang, R. Winston, Tracking control of high-concentration photovoltaic systems for minimizing power losses, Progress in Photovoltaics: Research and Applications (2012).